Active remote detection of radioactivity based on electromagnetic signatures

P. Sprangle, B. Hafizi, H. Milchberg, G. Nusinovich, and A. Zigler

Citation: Physics of Plasmas (1994-present) **21**, 013103 (2014); doi: 10.1063/1.4861633
View online: http://dx.doi.org/10.1063/1.4861633
View Table of Contents: http://scitation.aip.org/content/aip/journal/pop/21/1?ver=pdfcov
Published by the AIP Publishing

Active remote detection of radioactivity based on electromagnetic signatures

P. Sprangle,[1,2] B. Hafizi,[1] H. Milchberg,[2] G. Nusinovich,[2] and A. Zigler[2,3,4]
[1]*Plasma Physics Division, Naval Research Laboratory, Washington, District of Columbia 20375, USA*
[2]*University of Maryland, College Park, Maryland 20742-4111, USA*
[3]*Icarus Research, Inc., PO Box 30780, Bethesda, Maryland 20824-0780, USA*
[4]*The Hebrew University of Jerusalem, Jerusalem, Israel*

(Received 24 July 2013; accepted 23 December 2013; published online 14 January 2014)

This paper presents a new concept for the remote detection of radioactive materials. The concept is based on the detection of electromagnetic signatures in the vicinity of radioactive material and can enable stand-off detection at distances greater than 100 m. Radioactive materials emit gamma rays, which ionize the surrounding air. The ionized electrons rapidly attach to oxygen molecules forming O_2^- ions. The density of O_2^- around radioactive material can be several orders of magnitude greater than background levels. The elevated population of O_2^- extends several meters around the radioactive material. Electrons are easily photo-detached from O_2^- ions by laser radiation. The photo-detached electrons, in the presence of laser radiation, initiate avalanche ionization which results in a rapid increase in electron density. The rise in electron density induces a frequency modulation on a probe beam, which becomes a direct spectral signature for the presence of radioactive material.
[http://dx.doi.org/10.1063/1.4861633]

I. INTRODUCTION

Radioactive materials emit gamma rays, which ionize the surrounding air producing free electrons which rapidly attach to oxygen molecules forming O_2^- ions. The density of negative ions is far greater than the free electron density.[1,2] This is true even for ambient levels of radioactive material.

A recently proposed radioactivity detection concept is based on a high power THz pulse inducing avalanche breakdown and spark formation in the vicinity of the radioactive material.[3–6] In that concept, a THz pulse is focused to a volume V_{focal} near the radioactive material. In the absence of the radioactive material, the electron density N_e is sufficiently small so that $N_e V_{focal} \ll 1$. In this case, the probability of an electron appearing in the focal volume during the THz pulse is negligible, and the breakdown probability is very low. In the presence of radioactivity, however, $N_e V_{focal} \geq 1$, which will lead to avalanche ionization in the volume V_{focal} occurs provided the THz pulse intensity is above a threshold level and the pulse length is sufficiently long. Breakdown and spark formation requires that the collisional ionization rate exceed the attachment rate. A THz-based radioactivity detection concept may have unique advantages depending on the stand-off distance and atmospheric conditions.

In this paper, we propose and analyze an alternative detection concept using a high intensity laser beam and probe beam to detect electromagnetic signatures in the vicinity of radioactive material. Propagation of high power short pulse lasers in the atmosphere over extended distances has been analyzed[7] and experimentally characterized.[8–10] It is possible to arrange for the radiation beams to come to a focus in the vicinity of the radioactive material by making use of longitudinal compression and transverse focusing.[7] The negative ions produced by the radioactive material have an electron affinity resulting in a low ionization potential of 0.46 eV and can be photo-detached by laser radiation (~0.8–1 μm). Our detection approach is based on a probe radiation beam undergoing a frequency modulation while propagating in a temporally increasing electron density. The frequency modulation on the probe beam becomes a spectral signature for the presence of radioactive material. As with all detection concepts, the effectiveness of our approach depends on the level of shielding around the radioactive material. The level of shielding will determine the sensitivity of our concept. A schematic of the detection concept is shown in Fig. 1.

II. RADIOACTIVITY DETECTION CONCEPT

In Subsections II A–II C, the various elements of the detection concept are discussed and analyzed. Details of the analytical model are presented in the Appendix.

A. Radiation enhancement factor

A gamma ray propagating through matter can interact through several processes, including Rayleigh scattering, photoelectric and Compton effects, pair production, etc.[11] In air, photoelectric absorption dominates at low photon energies (<25 keV) while at high energies (~25 keV–3 MeV) Compton processes dominate. As the gamma ray propagates in air, it loses energy in a cascading process and its mean free path L_γ decreases. Gamma rays having energies of 1 MeV, 50 keV, 25 keV, or 10 keV, have mean free paths in air of $L_\gamma \approx 130$ m, 38 m, 19 m, or 1.9 m, respectively. Note that values for the range indicated here apply to the case where a gamma ray with the given energy is completely absorbed in a single interaction (collision). The actual mean

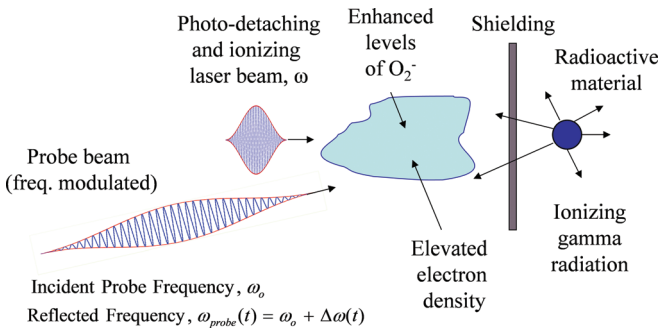

FIG. 1. Schematic of active remote radioactivity detection concept. Laser radiation photo-detaches electrons from O_2^- ions, providing electrons for an avalanche (collisional) ionization process which increases the electron density. A probe beam in the presence of a temporally increasing electron density undergoes a frequency modulation which becomes a spectral signature of radioactivity.

free path for a given initial energy is somewhat less than that for a single interaction.

The ionization rate due to background (ambient) radioactivity is $(dN_e/dt)_{amb} = Q_{rad}$. At or near ground level, the background ionization rate is typically in the range $Q_{rad} \sim$ 10–30 pairs/(cm^3–s). The gamma rays emitted by radioactive material ionize the surrounding air. In the presence of radioactive material, the ionization rate (due to only radiation) can be greatly enhanced by a factor $\alpha_{rad} \gg 1$ and $(dN_e/dt)_{rad} = \alpha_{rad} Q_{rad}$. Various air chemistry processes such as attachment and recombination limit the electron density and are discussed later and in the appendix.

The enhancement factor α_{rad} can be estimated as follows. For a radioactive material of mass M_{rad}, the number of disintegrations per second is $\nu_{rad} = M_{rad} A_{rad}$, where A_{rad} is the specific activity associated with the material. For example, for ^{60}Co, $A_{rad} = 1.1 \times 10^3$ Ci/g $= 4.1 \times 10^{13}$ disintegration/(g–s), where a Ci (Curie) is 3.7×10^{10} disintegrations/s. In the case of ^{60}Co, each disintegration results in two gammas of energy $E_{\gamma,\max} = 1.173$ MeV and $E_{\gamma,\max} = 1.332$ MeV, which have a range in air of ~130 m. In air, the high energy gammas generate high energy electrons, via Compton and photoelectric processes, which undergo a cascading process to sufficiently low energy to attach to O_2 molecules forming O_2^- ions. In the cascading process, the electrons lose an amount of energy $\Delta E \approx 35$ eV per collision in air, which results in both ionization and electronic excitation (~equal amounts of energy lost to each process).[12] A high energy electron with energy E_e therefore generates $\sim E_e/\Delta E$ low energy electrons. In the case of Compton absorption, the maximum electron energy is $E_e = (2\alpha_\gamma/(1+2\alpha_\gamma))E_{\gamma,\max}$, where $\alpha_\gamma = E_{\gamma,\max}/mc^2$. For example, a 1 MeV gamma ray in air generates Compton electrons having a maximum energy of $E_e = 0.8$ MeV and average energy of $\langle E_e \rangle = 0.44$ MeV. It should be noted that the range of high energy electrons is much less than the range of the high energy gammas. For example, an electron having energy of 1, 0.5, or 0.1 MeV has a range in air of 4.6, 3, or 2.1 m, respectively. Here again, as with the gamma rays mentioned earlier, the above electron ranges corresponds to the case where an electron is completely stopped in one interaction (collision).

For a small spherical source of radioactivity the steady state density of emitted gamma rays is

$$N_\gamma = \frac{\nu_{rad}\kappa_\gamma}{4\pi c R^2}\exp(-R/L_\gamma), \tag{1}$$

where R is the distance from the radioactive material, L_γ is the effective range (mean free path) of the gamma rays in air, which is a function of the gamma ray energy, E_γ, and κ_γ is the number of gammas emitted per disintegration. The rate of change of electron density is given by

$$\frac{\partial N_e}{\partial t} \approx (\alpha_{rad}+1)\,Q_{rad} + \text{air chemistry and ionization terms}, \tag{2}$$

where

$$\alpha_{rad} \approx c\langle\sigma_{\gamma-e}\rangle N_{air} N_\gamma \frac{\langle E_e\rangle}{\Delta E}\frac{1}{Q_{rad}} \approx \frac{\nu_{rad}\kappa_\gamma}{4\pi\langle L_{\gamma-e}\rangle}\frac{\langle E_e\rangle}{\Delta E}\frac{1}{Q_{rad}}\frac{\exp(-R/L_\gamma)}{R^2} \tag{3}$$

is the radiation enhancement factor. An equivalent result defining the detectable mass of the radioactivity material as a function of the various parameters was obtained in Ref. 6.

In the absence of radioactive material, $\alpha_{rad} = 0$. In Eq. (3) $\langle\sigma_{\gamma-e}\rangle = \langle\sigma_{\gamma-e}\rangle_{CA} + \langle\sigma_{\gamma-e}\rangle_{PE}$ is the effective average cross section for electron generation by gammas, i.e., Compton absorption and photoelectric processes, $\langle L_{\gamma-e}\rangle = \left(\langle\sigma_{\gamma-e}\rangle N_{air}\right)^{-1}$ is the average mean free path for electron generation by gammas and $N_{air} = 2.7 \times 10^{19}$ cm^{-3} is the air density (Loschmidt's number) at STP. The cross section $\sigma_{\gamma-e}(E)$ is a function of the gamma ray energy and the average cross-section is given by $\langle\sigma_{\gamma-e}\rangle = \int dE f(E)\,\sigma_{\gamma-e}(E)$, where $f(E)$ is the gamma ray energy distribution function. Over the range of energies ~0.05–1 MeV, Compton absorption dominates and $\langle\sigma_{\gamma-e}\rangle_{CA} \sim 1.4 \times 10^{-24}$cm^2, while for energies below ~0.05 MeV the photoelectric effect dominates with $\langle\sigma_{\gamma-e}\rangle_{PE}$ increasing from $\sim 1.4 \times 10^{-24}$ cm^2 at 0.05 MeV to $\sim 2 \times 10^{-22}$ cm^2 at 0.01 MeV. In Fig. 2, the radiation enhancement factor α_{rad} is plotted as a function of the distance from the radioactive source, R. This plot is for samples containing 1 mg and 10 mg of ^{60}Co and indicates that the enhanced level is significant for ranges extending up to several meters. As an example, for $\langle E_e\rangle = 0.5$ MeV, $M_{rad} = 10$ mg, $\nu_{rad} = M_{rad} A_{rad} = 8.2 \times 10^{11}$ disintegrations/s, $\kappa_\gamma = 2$, $R = 50$ cm, $\langle L_{\gamma-e}\rangle = 100$ m, and $Q_{rad} = 20$ disintegrations/(cm^3 – s), the radiation enhancement factor is $\alpha_{rad} \approx 2 \times 10^6$, which is far above the background level.

B. Electron and ion density evolution (air chemistry)

To determine the frequency modulation on a probe pulse, it is necessary to follow the time evolution of the electron and negative ion density, which are sensitive functions of air chemistry processes[13] and electron heating by the laser radiation. The source terms for the electrons include

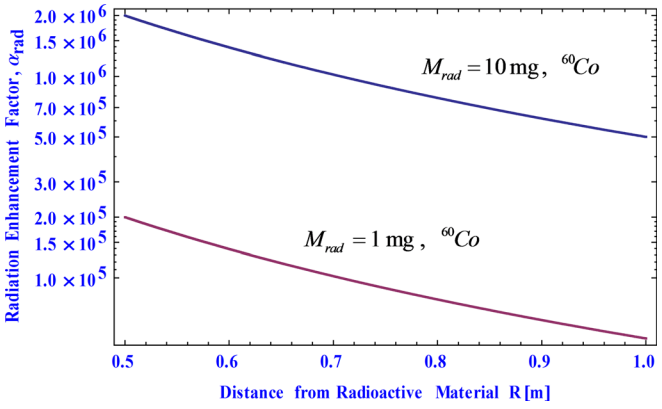

FIG. 2. Radiation enhancement factor plotted as a function of distance from the radioactive source for 1 mg and 10 mg of ^{60}Co.

radioactivity, detachment, photo-detachment and photo-ionization, while the loss terms include various attachment and recombination processes including aerosols. The expressions for the rate of change of electron density N_e and negative ion density N_- are[14–17]

$$\partial N_e/\partial t = (1+\alpha_{rad})Q_{rad} + S_e - L_e, \tag{4a}$$

$$\partial N_-/\partial t = S_- - L_-, \tag{4b}$$

where S_e represents the various electron source terms, L_e is the electron loss terms, S_- represents the ion source, L_- is the ion loss terms. The various source and loss terms are discussed in the appendix.

The effect of radioactivity is represented by the first term on the right hand side of the electron rate equation (4a). Since the free electron density is generally much less than the ion density, $N_e \ll N_-$ the steady state electron and negative ion densities are found to be given by $N_e \approx (\beta_n N_n/\eta)\sqrt{(1+\alpha_{rad})\,Q_{rad}/\beta_+} + (1+\alpha_{rad})\,Q_{rad}/\eta \approx (\beta_n N_n/\eta)\sqrt{(1+\alpha_{rad})\,Q_{rad}/\beta_+}$, and $N_- \approx \sqrt{(1+\alpha_{rad})\,Q_{rad}/\beta_+}$,[4] where N_n is the neutral air density ($N_n \sim N_{air}$ for low levels of ionization), $\beta_+ \approx 2\times10^{-6}\ \mathrm{cm^3/s}$ is the recombination rate, $\eta \approx 10^8\ \mathrm{s^{-1}}$ is the attachment rate, and $\beta_n \approx (5\text{–}10)\times10^{-19}\ \mathrm{cm^3/s}$ is the negative ion detachment rate due to collisions with neutrals (see appendix for details). In the absence of radioactive material ($\alpha_{rad}=0$) the ambient (background) electron and negative ion density are $N_e \approx 10^{-3}\ \mathrm{cm^{-3}}$ and $N_- \approx 3\times10^3\ \mathrm{cm^{-3}}$, where $Q_{rad} = 20\,\mathrm{cm^{-3}\,sec^{-1}}$. At a distance of 4 m from a radioactive source containing 10 mg of ^{60}Co, the radioactive enhancement factor is $\alpha_{rad} = 2.2\times10^4$ and the elevated electron and negative ion densities are $N_e \approx 0.2\,\mathrm{cm^{-3}}$ and $N_- \approx 4.7\times10^5\,\mathrm{cm^{-3}}$.

The various source and loss terms in Eqs. (4a) and (4b), in particular, the collisional ionization rate, are functions of the electron temperature (see Appendix). The electron temperature is determined by the collisional electron heating (Ohmic heating) by the laser radiation and the cooling effect resulting from excitation of vibrational modes of the air molecules. The equations for the electron temperature T_e is[18]

$$(3/2)\,\partial(N_e T_e)/\partial t = \langle \mathbf{J}\cdot\mathbf{E}\rangle - (3/2)(N_e/\tau_{cool})(T_e - T_{eo}), \tag{5}$$

where $\langle \mathbf{J}\cdot\mathbf{E}\rangle$ is the Ohmic heating rate, τ_{cool} is the electron cooling time due to inelastic collisions (see Appendix), $T_{eo} = 0.025\,\mathrm{eV}$ is the ambient electron room temperature. The heating and cooling terms on the right hand sides of Eq. (5) are discussed in the appendix.

C. Frequency modulation on a probe beam

A probe beam propagating through a region of space in which the electron density is changing with time will undergo a frequency change. The electron density in the vicinity of the radioactive source and under the influence of the laser radiation varies in space and in time. Consequently the frequency/wavenumber of an electromagnetic probe beam propagating in such plasma will vary in space and in time. The one-dimensional wave equation $(\partial^2/\partial z^2 - c^{-2}\partial^2/\partial t^2)A(z,t) = c^{-2}\omega_p^2(z,t)A(z,t)$ can be used to determine the frequency/wavenumber shift. Here, $\omega_p(z,t) = (4\pi q^2 N_e(z,t)/m)^{1/2}$ is the plasma frequency and $A(z,t)$ is the vector potential associated with the probe. The vector potential can be expressed in terms of slowly varying amplitude and phase, in the form $A(z,t) = (1/2)B(z,t)\exp[i(k_o z - \omega_o t) + i\theta(z,t)] + c.c.$, where ω_o is the incident probe frequency and $\theta(z,t)$ is the phase. The frequency of the probe is $\omega_{probe}(z,t) = \omega_o - \partial\theta(z,t)/\partial t$, where the phase θ satisfies $(\partial/\partial z + c^{-1}\partial/\partial t)\,\theta(z,t) = -\omega_p^2(z,t)/(2\omega_o c)$. The solution is $\theta(\eta,\tau) = -(2\omega_o c)^{-1}\int_0^{\eta\le L} d\eta'\,\omega_p^2(\eta', \tau+\eta'/c)$ where $\eta = z$, $\tau = t - z/c$, and L is the probe beam's interaction length. Since the phase $\theta(\eta,\tau)$ varies with time, it represents a shift in the frequency of the probe beam, which is measurable and is used as a signature of radioactivity. The frequency shift on the probe is $\Delta\omega(\eta,\tau) = -\partial\theta(\eta,\tau)/\partial\tau$. In particular, if the electron density is increasing with time the probe frequency will be increased. For a spatially uniform, temporally varying plasma density, the frequency shift on the probe beam is

$$\Delta\omega(z,t) = (2\omega_o)^{-1}(\omega_p^2(t) - \omega_p^2(t - z/c)), \tag{6}$$

where $0 \le z \le L$.

As an illustration, we consider the case where the rise in electron density is exponential in time and spatially uniform within a region $0 \le z \le L$. Here the plasma frequency is given by $\omega_p^2(z,t) = \omega_{po}^2\exp(\nu_{ion}t)\,g(z)$, where ν_{ion} is the effective ionization rate and $g(z) = 1$, $0 \le z \le L$, defines the axial extent of the plasma region. The frequency modulation on the probe beam is given by $\omega_{probe}(z,t) = \omega_o + \Delta\omega(z,t)$, where

$$\Delta\omega(z,t) = \omega_{po}^2/(2\omega_o)\exp(\nu_{ion}t)\,(1 - \exp(-\nu_{ion}\,z/c)). \tag{7}$$

The maximum fractional frequency shift occurs for $z > c/\nu_{ion} \sim 1\,\mathrm{cm}$ and is $\Delta\omega_{\max}/\omega_o = (\omega_{po}^2/2\omega_o^2)\exp(\nu_{ion}\,t)$. The effective ionization rate can vary widely but is typically $\nu_{ion} \sim 10^{11}\ \mathrm{s^{-1}}$. The frequency modulation on the probe beam can be substantial and is readily measurable.

III. RADIOACTIVITY DETECTION EXAMPLE

To illustrate the radioactivity detection concept, i.e., the frequency modulation induced on a probe beam by ionizing the air near the radioactive material, we consider the following example. In the numerical examples, the system quantities, i.e., electron density, ion density, electron temperature and frequency modulation on a probe laser, are calculated both in the absence ($\alpha_{rad} = 0$) and in the presence of radioactive material by numerically solving Eqs. (4)–(6). The radioactive source is assumed strong enough to produce a radiation enhancement factor of $\alpha_{rad} = 10^3$. The radiation enhancement factor value is consistent with low quantities of radioactive material as shown in Fig. 2. We take the ionizing laser to have a peak intensity of $I_{peak} = 160\,\mathrm{GW/cm^2}$ and pulse duration of $\tau_{laser} = 1\,\mathrm{ns}$. In these examples, the probe beam is taken to be a millimeter wave source of frequency $f_{probe} = 94\,\mathrm{GHz}$, ($\lambda_{probe} = 3.2\,\mathrm{mm}$). The critical electron density, associated with the probe frequency, $\omega_{probe} = \omega_{p,crit} = 5.64 \times 10^4 n_{e,crit}^{1/2}[\mathrm{cm^{-3}}]$, is $n_{e,crit} = 10^{14}\,\mathrm{cm^{-3}}$. The background radiation is taken to be $Q_{rad} = 30$ disintegrations/($\mathrm{cm^3}$–s).

In the absence of radioactivity the ionizing laser intensity is just below the breakdown level, i.e., the electron density is low, Fig. 3(a), and there is virtually no frequency modulation on the probe beam. Figure 3(b) shows the electron density as a function of time in the presence of radioactive material ($\alpha_{rad} = 10^3$). The electron density at the end of the ionizing laser pulse approaches the value of $n_e = 10^{13}\mathrm{cm^{-3}}$, which is an order of magnitude less than the critical electron density.

The frequency modulation on the probe millimeter wave beam is shown in Fig. 4. In the absence of radioactive material, there is no frequency modulation on the probe. However, for $\alpha_{rad} = 10^3$, the fractional frequency modulation is significant and equal to ~5 %, which is readily detectable.

The fractional frequency shift on the probe as a function of both axial interaction distance L and time is shown in Fig. 5.

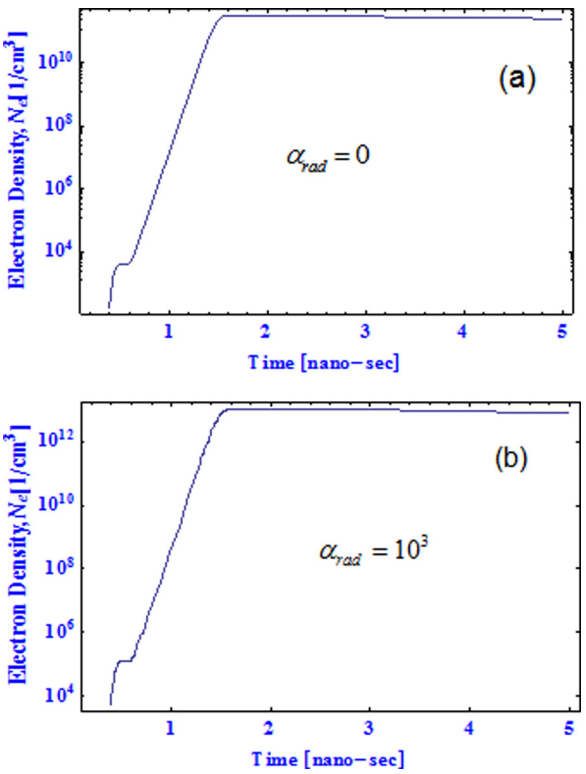

FIG. 3. Electron density as a function of time, (a) no external radioactivity ($\alpha_{rad} = 0$), (b) in the presence of radioactivity ($\alpha_{rad} = 10^3$). The laser parameters are, $\lambda = 1\,\mu\mathrm{m}$, $I_{peak} = 160\ \mathrm{GW/cm^2}$ and $\tau_{laser} = 1\,\mathrm{ns}$.

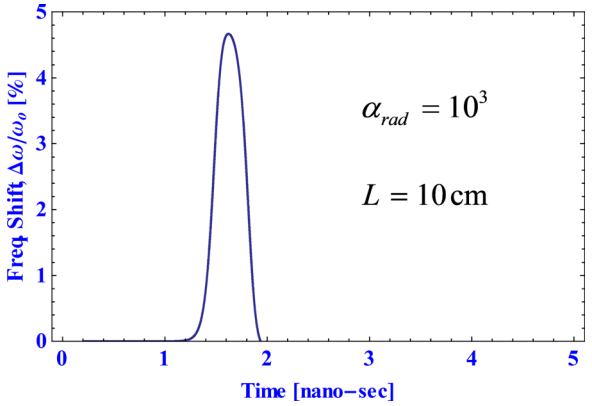

FIG. 4. Fractional frequency shift $\Delta\omega/\omega_o$ [%] versus time in the presence of radioactive material $\alpha_{rad} = 10^3$ at the probe interaction distance of $L = 10\,\mathrm{cm}$. The laser parameters are the same as in Fig. 3(b).

IV. DISCUSSION AND SUMMARY

In this paper, a concept is proposed and analyzed for active remote detection of radioactive materials. The enhanced levels of ionization associated with the presence of radioactivity may be detected using a combination of an ionizing laser and probe beam. The detection concept depends on the fact that the free electrons produced by gamma rays emitted by the radioactive material attach rapidly to oxygen molecules forming negative ions O_2^-. In the vicinity of radioactive material, the density of negative ions is elevated compared to the background density, while the free electron density remains extremely low. The negative oxygen ions can be readily photo-detached with laser radiation. The photo-detached electrons, in the presence of the laser radiation, initiate an avalanche ionization process, which greatly increases the electron density. To detect this change in electron density, a probe beam is

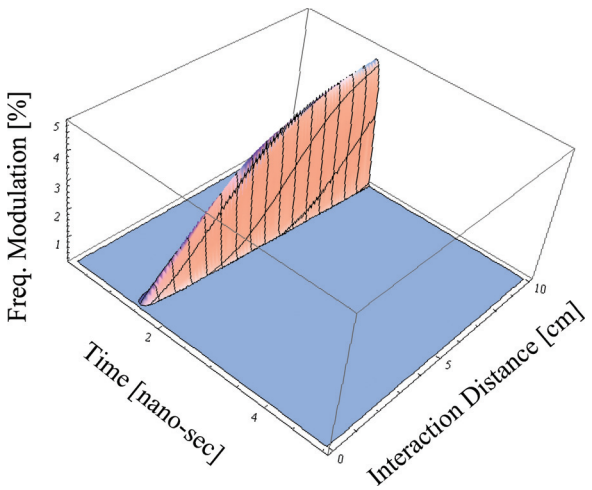

FIG. 5. Fractional frequency shift $\Delta\omega/\omega_o$ [%] versus time and probe interaction distance L in the presence of radioactive material ($\alpha_{rad} = 10^3$). The laser parameters are the same as in Fig. 3(a).

employed. The probe beam undergoes frequency modulation in the presence of the temporally changing electron density. The frequency modulation on the probe beam is a signature of the presence of radioactive material. Our analysis indicates that a measurable frequency shift can be expected for relatively small amounts of radioactive material.

Plans are underway to experimentally demonstrate this detection concept at the University of Maryland. The experiments employ a commercial source of alpha particles to simulate the nuclear material. Note that in an actual detection device, gammas not alphas would provide the initial negative ions. The nuclear material is ^{210}Po, producing 5 MeV alpha particles. Using a radioactive source of alphas in place of a gamma ray source avoids the safety issues associated with radioactive material. Note that 5 MeV alphas have a short range ($\sim$3.5 cm) in air. The commercial source produces 20 mCi of radioactivity from ^{210}Po inside an open metallic tube. Each 5 MeV alpha will generate $\sim 1.4 \times 10^5$ electrons which attach to O_2 forming O_2^- ions. The O_2^- ions are blown out of the tube and are photo-detached by laser radiation.

The photo-detaching and ionizing beam in the experiments is a Nd:YAG, 5 GW, 100 ps laser. The diagnostics include visible and extreme ultraviolet spectrometers, interferometers for measuring electron density profiles, microwave and ultrafast pulse diagnostics. The probe beam used in these experiments is a 30 GHz, circularly polarized continuous wave microwave source. Focusing the laser radiation near the ^{210}Po source photo-detaches the negative ions and initiates an avalanche ionization process. The temporal rise in electron density produces a detectable frequency modulation on the probe beam.

The purpose of this paper is to present a new concept for the detection of radioactive material. Our analysis indicates that a measurable frequency modulation on a probe beam is induced even in the presence of small quantities of radioactive material. A more rigorous analysis requires a more detailed model of the air chemistry processes.

ACKNOWLEDGMENTS

The authors acknowledge useful discussions with Dr. Victor Granatstein and Dr. Carlos Romero-Talamas. The authors also acknowledge useful discussions concerning the air chemistry model with Dr. Richard Fernsler and Dr. Steven Slinker. This work was supported by NRL 6.1 base funds and by the Office of Naval Research.

APPENDIX: AIR CHEMISTRY AND IONIZATION RATES

1. Electron and ion density dynamics

The rate of change of electron density N_e and the negative ion density N_-, Eqs. (4a) and (4b), are given by

$$\partial N_e/\partial t = \alpha_{rad} Q_{rad} + S_e - L_e, \tag{A1}$$

$$\partial N_-/\partial t = S_- - L_-, \tag{A2}$$

and the source and loss terms are given by

$$S_e = \nu_{coll} N_e + \nu_{opt} N_- + \beta_- N_- N_e + \beta_n N_n N_-, \tag{A3}$$

$$L_e = \beta_e N_+ N_e + \eta N_e + \beta_{Ae} N_A N_e, \tag{A4}$$

$$S_- = \eta N_e, \tag{A5}$$

$$L_- = \beta_+ N_+ N_- + \beta_n N_n N_- + \nu_{opt} N_- + \beta_- N_- N_e + \beta_{A-} N_A N_-, \tag{A6}$$

and the positive ion density is given by $N_+ = N_e + N_-$ (charge neutrality). In air, the negative ion population is mainly O_2^-. In these equations N_n is the neutral air density, N_A is the density of aerosols, ν_{coll} is the collisional ionization rate, ν_{opt} is the photo-detachment rate, $\beta_e \sim 3 \times 10^{-8}\,\mathrm{cm^3\,s^{-1}}$ is the electron-ion dissociative recombination rate, $\beta_n = (5\text{–}10) \times 10^{-19}\,\mathrm{cm^3\,s^{-1}}$ is the negative ion detachment rate due to collisions with neutrals, $\eta \sim 10^8\,\mathrm{s^{-1}}$ is the electron attachment rate, $\beta_+ \sim 2 \times 10^{-6}\,\mathrm{cm^3\,s^{-1}}$ is the negative ion recombination rate, β_{A-} is the aerosol-ion attachment rate and β_{Ae} is the aerosol-electron attachment rate, ν_{coll} is the collisional ionization rate, and β_- is the negative ion detachment rate due to collisions with electrons. The various attachment and recombination rates are complicated functions of the system parameters, in particular the electron temperature. In our model, we approximate the various attachment and recombination rates as constants given by the above values. For example the negative ion detachment rate due to collisions with neutrals is estimated as $\beta_n = \sigma \mathrm{v}_{O_2^-} \exp(-U_{aff}/T)$ where $\sigma\,(\approx 10^{-15}\,\mathrm{cm^2})$ is the elastic collision cross-section, $\mathrm{v}_{O_2^-}$ is the O_2^- thermal speed and U_{aff} (0.46 eV) is the electron affinity.

2. Photo-detachment of O_2^-

The electron affinity of O_2^- is 0.46 eV and therefore can undergo single-photon photo-detachment with laser radiation of wavelength $\lambda = 1\,\mu$m (1.24 eV) or $\lambda = 0.8\,\mu$m (1.55 eV). The photo-detachment rate is $\nu_{opt} = \sigma_{opt} c N_{ph} = \sigma_{opt} I_o/\hbar\omega$, where $cN_{ph} = I_o/\hbar\omega$ is the incident photon flux, I_o is the laser intensity and σ_{opt} is the photo-detachment cross section. The experimental value for the single-photon photo-detachment cross section of O_2^- is $\sigma_{opt}(\lambda = 1\,\mu\mathrm{m}) \approx 4.5 \times 10^{-19}\,\mathrm{cm^2}$ and $\sigma_{opt}(\lambda = 0.8\,\mu\mathrm{m}) \approx 7.5 \times 10^{-19}\,\mathrm{cm^2}$.[16] The single-photon photo-detachment rate for O_2^- is therefore

$$\nu_{opt}[\mathrm{sec^{-1}}] = I_o[\mathrm{W/cm^2}] \begin{cases} 2.3, & \lambda = 1\,\mu\mathrm{m} \\ 3, & \lambda = 0.8\,\mu\mathrm{m}. \end{cases} \tag{A7}$$

For the parameters considered here, multiphoton ionization of air can be neglected since the ionization potential for clean air (O_2) is $\sim$12 eV and requires $\sim$8–10 photons.

3. Collisional (avalanche) ionization of air

The collisional ionization rate is given by $\nu_{coll} = N_{air} \int_{\mathrm{v}_I}^{\infty} d\mathrm{v} \sigma_{coll}(\mathrm{v})\,\mathrm{v} f_e(\mathrm{v})$, where σ_{coll} is the collisional ionization cross section and $f_e(\mathrm{v})$ is the electron distribution function is taken to be a Maxwellian, with $\int d\mathrm{v} f_e = 1$. The cross section can be approximated near the threshold by $\sigma_{coll} \approx C\,(\varepsilon - U_I)$ where $\varepsilon = m\mathrm{v}^2/2$ is the electron energy, U_I is the ionization energy, $\mathrm{v}_I = (2U_I/m)^{1/2}$, and C is a constant associated with

the molecule. The collisional ionization rate in air can be written in the form $\nu_{coll} = \nu_{coll}(N_2) + \nu_{coll}(O_2)$ where the ionization rates of N_2 and O_2 have the form

$$\nu_{coll}(X) = \nu_X \left(T_e/U_X\right)^{3/2} \left(U_X/T_e + 2\right) \exp(-U_X/T_e), \quad \text{(A8)}$$

with $U_{N_2} = 15.6$ eV, $U_{O_2} = 12.1$ eV and, at STP, $\nu_{N_2} = 7.6 \times 10^{11}\ s^{-1}$, and $\nu_{O_2} = 10^{11}\ s^{-1}$.[18]

4. Electron cooling rate

The various inelastic electron cooling processes in air are complicated and include excitation of vibrational, rotational and electronic states.[19] At low electron energies the dominant inelastic cooling processes is the excitation of vibrational states of N_2. As the electron temperature increases, the electron cooling rate increases due to collisional excitation of the nitrogen molecule vibrational states. We model the inelastic electron cooling rate as $1/\tau_{cool} = (2/3)(2m/M_{eff})^{eff}\,\nu_e$, where M_{eff} is the effective molecular mass and the electron collision frequency ν_e is the sum of the electron-neutral and electron-ion contributions, $\nu_e = \nu_{en} + \nu_{ei}$, with $\nu_{en}[s^{-1}] \approx 10^{-7} N_n\,[cm^{-3}]\, T_e^{1/2}[eV]$ and $\nu_{ei}[s^{-1}] \approx 10^{-5} N_e\,[cm^{-3}]\, T_e^{-3/2}[eV]$. In the computations the effective molecular mass M_{eff} is taken to be 200 in order to obtain the correct breakdown field for ionization with 10.6 μm and 1.06 μm lasers. For the parameters of interest here the plasma is weakly ionized and electron-ion collisions are negligible compared to electron-neutral collisions.

5. Electron heating

The collisional electron heating term $\langle \mathbf{J} \cdot \mathbf{E} \rangle$ in Eq. (5) is obtained by representing the laser field and electron current density by $\mathbf{E} = E_o(z,t)\exp(i\Psi(z,t))\,\hat{\mathbf{e}}_x/2 + \text{c.c.}$ and $\mathbf{J} = J_o(z,t)\exp(i\Psi(z,t))\,\hat{\mathbf{e}}_x/2 + \text{c.c.}$, respectively, where $\Psi = \omega(z/c - t)$, $J_o(z,t) = iq^2 N_e(z,t)\,(E_o(z,t)/m)/(\omega + i\,\nu_e(z,t))$, $E_o[V/cm] = 27.4 I_o^{1/2}[W/cm^2]$ is the laser field amplitude, $I_o = c|E_o|^2/8\pi$ is the intensity, ω is the laser frequency, $\hat{\mathbf{e}}_x$ is a unit polarization vector along the x- axis, and c.c. denotes the complex conjugate. The electron current density and field are related by $\partial\mathbf{J}/\partial t + \nu_e\mathbf{J} = (\omega_p^2/4\pi)\mathbf{E}$, where $\omega_p = (4\pi q^2 N_e/m)^{1/2}$ is the plasma frequency. The time-average rate of change of electron energy density is $\langle \mathbf{J}\cdot\mathbf{E} \rangle = (\omega_p^2/8\pi)E_{eff}^2/\nu_e$, where $E_{eff} = (\nu_e/\omega)/\,(1+\nu_e^2/\omega^2)^{1/2} E_o$ is the effective laser electric field. In practical units

$$\langle \mathbf{J} \cdot \mathbf{E} \rangle\,[\text{eV-cm}^{-3}/\text{s}] = 1.9 \times 10^{-13}\, N_e[\text{cm}^{-3}]\, \lambda^2[\mu\text{m}] \times I_o[\text{W/cm}^2]\, \nu_e[\text{s}^{-1}]/(1 + \nu_e^2/\omega^2). \quad \text{(A9)}$$

Typically, for lasers, $\omega \gg \nu_e$ while for millimeter waves ω can be comparable to ν_e.

[1] W. A. Hoppel, R. V. Anderson, and J. C. Willett, *The Earth's Electrical Environment* (The National Academies Press, 1986), p. 149.
[2] A. J. Peurrung, Nucl. Instrum. Methods Phys. Res., Sect. A **481**, 731 (2002)
[3] V. L. Granatstein and G. S. Nusinovich, J. Appl. Phys. **108**, 063304 (2010)
[4] G. S. Nusinovich, P. Sprangle, C. R. Talamas, and V. L. Granatstein, J. Appl. Phys. **109**, 083303 (2011).
[5] G. S. Nusinovich, R. Pu, T. M. Antonsen, O. V. Sinitsyn, J. Rodgers, A. Mohamed, J. Silverman, M. Al-Sheikhly, Y. S. Dimant, G. M. Milikh, M. Yu, Glyavin, A. G. Luchinin, E. A. Kopelovich, and V. L. Granatstein, J. Infrared Millim. THz Waves **32**, 380 (2011).
[6] Y. S. Dimant, G. S. Nusinovich, P. Sprangle, J. Peñano, C. A. Romero-Talamas, and V. L. Granatstein, J. Appl. Phys. **112**, 083303 (2012).
[7] P. Sprangle, J. R. Peñano, and B. Hafizi, Phys. Rev. E **66**, 046418 (2002).
[8] A. Ting, I. Alexeev, D. Gordon, E. Briscoe, J. Penano, R. Fischer, R. Hubbard, P. Sprangle, and G. Rubel, Appl. Opt. **44**, 5315 (2005).
[9] S. Varma, Y.-H. Chen, and H. M. Milchberg, Phys. Rev. Lett. **101**, 205001 (2008).
[10] S. Eisenmann, J. Peñano, P. Sprangle, and A. Zigler, Phys. Rev. Lett. **100**, 155003 (2008).
[11] *American Institute of Physics Handbook, 3rd ed.*, edited by D. E. Gray (McGraw-Hill, New York, 1972), pp. 8–203.
[12] M. H. Rees, *Physics and Chemistry of the Upper Atmosphere* (Cambridge University Press, Cambridge, UK, 1989), p. 40.
[13] M. Capitelli, C. M. Ferreira, B. F. Gordiets, and A. I. Osipov, *Plasma Kinetics in Atmospheric Gases* (Springer-Verlag, NY, 2010).
[14] R. F. Fernsler, A. W. Ali, J. R. Greig, and I. M. Vitkovitsky, "The NRL CHMAIR Code: A Disturbed Sea Level Air Chemistry Code," NRL Memorandum Report No. 4110, 1979.
[15] A. W. Ali, "Electron Energy Loss Rates in Air," NRL Memorandum Report No. 5400, 1984.
[16] L. G. Christophorou, *Atomic and Molecular Radiation Physics* (Wiley-Interscience, London, UK, 1971), p. 530.
[17] P. Sprangle, J. Peñano, B. Hafizi, D. Gordon, and M. Scully, Appl. Phys. Lett. **98**, 211102 (2011).
[18] Y. B. Zel'dovich and Y. P. Raizer, *Physics of Shock Waves and High-Temperature Hydrodynamic Phenomena* (Dover, Mineola, NY, 2002).
[19] R. Schunk and A. Nagy, *Ionospheres* (Cambridge University Press, Cambridge, UK, 2009).